

Separation of sperm cells from samples containing high concentrations of white blood cells using a spiral channel

Jiyoung Son,¹ Raheel Samuel,² Bruce K. Gale,³ Douglas T. Carrell,²
and James M. Hotaling²

¹*Department of Electrical and Computer Engineering, University of Utah, Salt Lake City, Utah 84112, USA*

²*Urology Division of Department of Surgery, University of Utah School of Medicine, Salt Lake City, Utah 84108, USA*

³*Department of Mechanical Engineering, University of Utah, Salt Lake City, Utah 84112, USA*

(Received 5 July 2017; accepted 24 August 2017; published online 27 September 2017)

Microfluidic technology has potential to separate sperm cells from unwanted debris while improving the effectiveness of assisted reproductive technologies (ART). Current clinical protocol limitations regarding the separation of sperm cells from other cells/cellular debris can lead to low sperm recovery when the sample contains a low concentration of mostly low motility sperm cells and a high concentration of unwanted cells/cellular debris, such as in semen samples from patients with pyospermia [high white blood cell (WBC) semen]. This study demonstrates label-free separation of sperm cells from such semen samples using inertial microfluidics. The approach does not require any externally applied forces except the movement of the fluid sample through the instrument. Using this approach, it was possible to recover not only any motile sperm, but also viable less-motile and non-motile sperm cells with high recovery rates. Our results demonstrate the ability of inertial microfluidics to significantly reduce WBC concentration by flow focusing of target WBCs within a spiral channel flow. The estimated sample process time was more rapid (~5 min) and autonomous than the conventional method (gradient centrifuge sperm wash; ~1 h). A mixture of sperm/WBC was injected as the device input and 83% of sperm cells and 93% of WBCs were collected separately from two distinct outlets. The results show promise for enhancing sperm samples through inertial flow processing of WBCs and sperm cells that can provide an advantage to ART procedures such as sample preparation for intrauterine insemination. *Published by AIP Publishing.*
[\[http://dx.doi.org/10.1063/1.4994548\]](http://dx.doi.org/10.1063/1.4994548)

INTRODUCTION

Microfluidic technology provides valuable options for cell sorting and separation, and can be used to replace tedious and inefficient conventional protocols.^{1–6} Of particular interest to us are research efforts related to microfluidic methods for separating sperm cells from unwanted debris while improving the efficiency of assisted reproductive technologies (ART). In one of the earliest such efforts, a glass microfluidic chip containing multiple microchannels connecting an input reservoir to a collecting reservoir enabled motile sperm cells to swim to specific reservoirs where they could be collected while removing non-motile sperm cells and debris.^{7,8} This technology first demonstrated the value of microfluidic platforms for sperm separation. More recently, a common microfluidic approach for sperm separation has been developed involving parallel laminar fluid streams of media through straight microchannels: one stream consists of a dilute semen sample and the other stream contains sperm media.^{9,10} At the microscale, the two fluid streams do not mix readily, so only motile sperm cells can travel across the interface between the two parallel streams. The two streams are separated again after a length sufficient to allow motile sperm cells to cross the boundary in high numbers, generating the separation of motile sperm cells from non-motile sperm cells and debris. Following a series of device

optimizations, the utility of this technology for ART was verified using sperm cells collected from the outlet for In vitro Fertilization (IVF).^{11–16} Another novel microfluidic approach to sperm separation utilizes chemotaxis in addition to motility. This approach induces sperm cells to travel through microchannels toward chemo-attractants which were applied to the bottom surface of the collection reservoirs at the periphery of the device.^{17–19}

Most of the sperm separation approaches utilizing microfluidics rely on sperm motility for separation with added features through which only highly motile sperm cells can pass: chemo-attractants, physical obstacles, and microdiffusers.^{7,8,17–27} Thus, these techniques can separate only progressive motile sperm cells from semen samples, but they lose a significant number of sperm cells including viable non-progressive motile and non-motile sperm cells, and are not feasible for use with immature and non-motile sperm cells that may be the only sperm cells produced by some patients. Thus, a system to recover all sperm cells, not just motile sperm cells, is needed. Such a device would serve a wide patient base needing sperm sample preparation.

Recently, we demonstrated sperm separation from a simulated microTESE sample, which included sperm cells, blood cells, and other debris,²⁸ using a passive, purely mechanical, label-free microfluidic approach based on inertial microfluidics that separated sperm cells (regardless of their motility state) from other unwanted cells/debris. The approach did not require any externally applied forces except the movement of the fluid sample through the instrument. The system could recover not only motile sperm cells, but also viable less-motile and non-motile sperm cells with high recovery rates. This study also suggested that a precisely designed spiral channel could generate some flow focusing of sperm cells, making it a suitable solution for increasing the purity of sperm cells from semen samples with high concentrations of unwanted particles, such as the high concentration of white blood cells (WBCs) in semen samples obtained from leukospermic patients.

Leukospermia is a condition characterized by abnormally high white blood cell (WBC) concentrations in semen ($>1 \times 10^6$ WBCs/milliliter of semen), which may lead to infertility and render ART procedures such as Intrauterine Insemination (IUI) ineffective. As highlighted by Gambera,²⁹ high concentrations of WBCs in the semen can cause disruption during fertilization. To deal with leukospermia, a density gradient centrifugation preparation method is widely utilized in fertility clinics as a WBC separation method. It consists of filtering sperm cells by centrifugal forces through either one or multiple layers of increasingly concentrated silane-coated silica particles. This process is able to generate a pellet at the bottom of the tube which contains a higher percentage of clean, motile sperm cells for IUI.³⁰ Mechanical filtration using physical filters such as micropore filters can also be used with leukospermic samples to separate sperm cells, but the filters readily clog due to the high number of WBCs and various random tissues in the sample.³¹ Unfortunately, all these methods lead to low sperm recovery when the starting sample has a low concentration of sperm cells.^{31,32} Additionally, centrifugal methods also require significant time (~ 1 h) to prepare the sample, which creates a potentially problematic time gap between sample preparation and insemination. Accordingly, there is a need for a clinical method with a high sperm recovery rate from samples with low sperm concentrations. Additionally, a sample preparation time reduction can provide significant relief to IUI patients who are under stress from the IUI procedure itself.

In this study, we demonstrate the use of inertial microfluidic technology to separate sperm cells from WBCs, the major contaminant in leukospermic semen samples, by flow focusing sperm cells and WBCs into different flow exits. This new method could conveniently process semen on-site in a clinic with much shorter processing times; ~ 10 times faster. The results show moderate sperm flow focusing and clear WBC flow focusing, indicating that this method can be used for sperm concentration enrichment even when working with high WBC concentrations or debris-filled semen samples (Fig. 1).

DESIGN AND THEORY

To enable the most effective and efficient WBC removal from a semen sample using a spiral channel, the appropriate dimensions of the spiral channel can be calculated based on

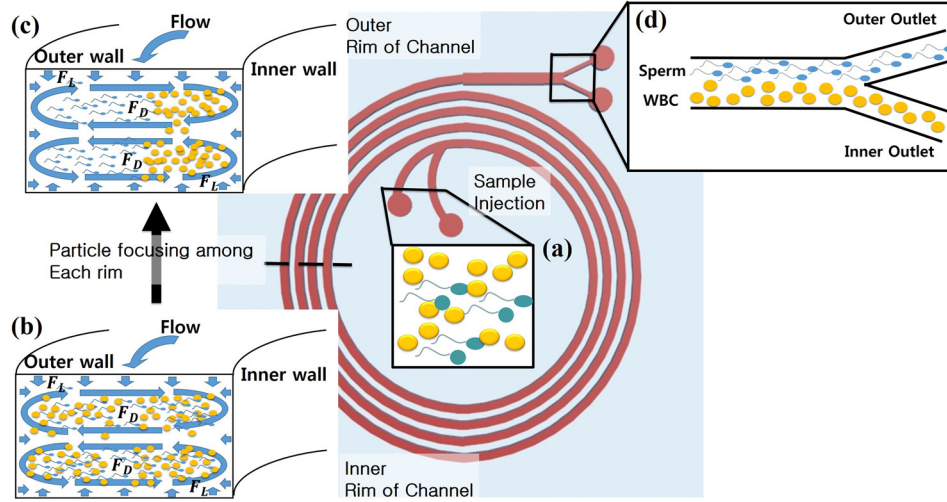


FIG. 1. An overview of the approach: a spiral channel is utilized to enrich pyospermic semen samples (high concentration of WBCs). (a) A semen sample with a high concentration of WBCs (yellow) and a low sperm (blue) concentration is injected through the inlets. (b) Evenly distributed cells at the first ring of the spiral. Flow focusing of particles in the channels proceeds as the sample moves through the spiral. (c) The lateral migration of each cell (sperm and WBC) continues until each cell reaches equilibrium positions in the later rings of the spiral. (d) Focused flow cells at the outlet area: most of the WBCs are collected at the inner outlet and sperm cells are collected at the outer outlet.

inertial microfluidic theory, which depends on the force ratio (R_f), the ratio of particle diameter and hydraulic diameter (λ), and the aspect ratio of the channel. The force ratio (R_f) is a ratio between the Dean drag force (F_D) and the lift force (F_L), all given by^{33,34}

$$R_f = \frac{F_L}{F_D} \geq \sim 0.08, \quad (1)$$

$$F_D = 3\pi\mu U_{Dean} a_p, \quad (2)$$

$$F_L = 0.05 \frac{a_p^4 \rho U_m^2}{D_h^2}, \quad (3)$$

where F_D is the force resulting from a secondary vortex that appears in the channel laterally due to Dean flow, F_L is the lift force that pushes all particles away from the channel walls, μ is the fluid viscosity, U_{Dean} is the average Dean velocity, a_p is the particle diameter, D_h is the hydraulic diameter of the channel, and U_m is the maximum fluid velocity. When R_f is higher than 0.08, the flow should be able to generate target particle focusing. The ratio λ [Eq. (4)]

$$\lambda = \frac{a_p}{D_h} \geq 0.07, \quad (4)$$

should be more than 0.07 to generate optimal particle focusing flow,³⁵ and the aspect ratio of the channel should be approximately between 0.5 and 0.25 (height/width),^{36,37} The channel length (L_l) required for a particle to reach its equilibrium position can be calculated by³³

$$L_l = \frac{U_f}{U_L} \times L_M, \quad (5)$$

where U_f is the flow velocity, U_L is the lateral migration velocity of the particle

$$U_L = 0.5 \frac{\rho U_m^2 a_p^3}{3\pi\mu D_h^2}, \quad (6)$$

and L_M is the migration length.

$$L_M = W + H + \frac{3}{4}W. \quad (7)$$

The target cell's dimensions, a_p in this case, can be approximated as a sphere having the largest diameter of each cell. The most common white blood cell (WBC) is the neutrophil, which is reported to have an average diameter of $12 \mu\text{m}$, and the longest sperm head dimension is about $5 \mu\text{m}$.^{38–41} Approximating cells as spheres to simplify calculations is reasonable based on an experimental study involving asymmetrical particle focusing within a microfluidic channel by Hur *et al.*⁴² This study suggests that the maximum diameter (rotational diameter) of an asymmetrical particle determines the stable position, and can be used to predict the movement of asymmetrical particles in spiral channels.

A range of dimensions and flow rates were used within the equations [Eqs. (1)–(4)] to find the best conditions for flow focusing (R_f , λ , and aspect ratio) and fabrication convenience. After a series of calculations, we found a set of dimensions which satisfied the design guidelines (ratio conditions from Eqs. (1) and (4): height = $50 \mu\text{m}$, width = $150 \mu\text{m}$, space between channels = $310 \mu\text{m}$, initial radius = $700 \mu\text{m}$, and final radius = $899 \mu\text{m}$). For the selected dimensions, $\lambda = 0.16$ for a $12 \mu\text{m}$ diameter particle and $\lambda = 0.067$ for a $5 \mu\text{m}$ diameter particle. The injection flow rate was selected based on the experimental results of our previous work.²⁸ Our previous report demonstrated the characterization of sperm cells and RBCs over a large range of flow rates (0.1 – 0.52 ml/min), and the flow focusing effect at 0.52 ml/min provided a reasonable flow focusing trend for sperm cells and a sharp flow focusing effect for RBCs. Since our goal is finding an alternative sperm concentration enhancement method, generating a sharp WBC flow focusing effect can achieve this goal effectively. Since WBCs are larger than RBCs (WBC $\sim 12 \mu\text{m}$, RBC $\sim 9 \mu\text{m}$) and the overall shape is closer to a sphere, there should be a sharp flow focusing effect like that for RBCs at 0.52 ml/min . Thus, 0.52 ml/min was chosen for most experiments. Note that the force ratio values for 0.52 ml/min are $= 0.40$ for $5 \mu\text{m}$ particles and 5.63 for $12 \mu\text{m}$ particles.

METHODOLOGY/EXPERIMENTAL

To demonstrate the separation capability of the spiral channel with sperm cells and WBCs, a series of experiments were designed to show the flow focusing of sperm cells and WBCs.

Fabrication of the designed device was carried out using polydimethylsiloxane (PDMS, Sylgard 184, Dow Corning, MI, USA) with a SU-8 (SU-8 3035, Microchem, MA, USA) mold. The SU-8 mold was fabricated on a 100 mm (4 in.) wafer according to the manufacturer's instructions in a clean room environment. 40 ml of uncured PDMS at a 10:1 (PDMS base:curing agent) ratio was poured over the mold, and it was placed in an oven at 60°C for at least 6 h . After curing, the molded PDMS was peeled off from the mold and any excess PDMS was removed. Inlets and outlets were cored with a 1.5 mm diameter coring tool. After cleaning the channel side surface of the PDMS piece, a glass slide (Corning 2947– $70 \times 50 \text{ mm}$) was plasma bonded with the PDMS to form a closed channel.

All sperm and WBC samples were acquired under an Institutional Review Board-approved study, IRB00072239. Written informed consent was obtained from all participants for their samples to be utilized for this study. Sperm samples were prepared from previously frozen semen specimens which were suspended in sperm media [Quinn's Advantage media with HEPES (Sage, CT, USA) and 3% of serum protein substitute (Sage, CT, USA)]. WBC samples were obtained from donor's whole blood specimens within one week of collection. Note that WBC samples mostly contained WBCs and small amounts of RBCs, because the WBC separation process from the whole blood could not separate RBCs completely. WBC samples were also suspended in the sperm media. The sperm and WBC samples were diluted using the sperm media to avoid concentration disturbances and we experimentally found the optimal total cell

TABLE I. Sample details. WBC A sample is for WBC characterization purposes, and Semen A represents simulated high WBC semen sample.

Sample type	WBC concentration (million/ml)	^a RBC concentration (million/ml)	Sperm concentration (million/ml)
WBC A	8.1	1.3	0
Semen A	8.35	1.4	2.45

^aRBC count data appeared in the table because WBCs were separated from a whole blood sample. Therefore, there were a small amount of RBCs in the WBC sample.

concentration range from a previous study:²⁸ <10 million cells/ml. Table I provides a technical description of each sample type and its label.

The prepared samples were placed within two 1 ml plastic syringes (BD, 1 ml Syringe Luer-lock tip), and each syringe was connected to the spiral channel inlets through platinum-cured silicone tubing (Sani-Tech, Clear Platinum-Cured Silicone Tubing, STHT-062-1) and nylon barbs (Nordson Medical, Straight Through Tube Fitting, N210-1). The outlet sample collection setup was constructed in the same manner as the inlet setup, and the separated samples from the two outlets were collected in two 1 ml plastic syringes (one for each outlet).

Samples were split into two syringes and injected through two spiral channel inlets using a dual syringe pump. Two inlets were used instead of one because it helped eliminate leaks near the inlet port, as found previously.²⁸ The injection flow rate was close to the calculated flow rate (0.26 ml/min from each syringe, resulting in an accumulated flow rate of 0.52 ml/min). To collect equal amounts of sample from each outlet, another set of two syringe pumps pulled the sample with a slightly lower flow rate than the injection flow rate (0.2 ml/min) to provide a back pressure and prevent gas bubble formation in the outlet area.

To observe and characterize the behavior of WBCs in the spiral channel, samples were prepared from two different donors and diluted to a concentration of 8.1×10^6 /ml (WBC A sample, Table I). The concentration was selected to simulate a high WBC concentration [WBC: $>1 \times 10^6$ /ml (Ref. 29)] in semen samples from pyospermic patients. The prepared WBC A sample was injected at 0.52 ml min^{-1} and collected from two outlets (inner and outer outlets).

Semen A sample was prepared by spiking WBC into semen;^{29,43} the cell concentrations were 2.45 and 8.35×10^6 /ml sperm cells and WBCs, respectively (Semen A sample, Table I). These concentrations were selected to simulate the extreme conditions of highly WBC contaminated semen with low sperm concentration. Prepared samples were injected at 0.52 ml min^{-1} . After processing with the spiral channel, the eluted material was collected from both outlets, and both WBCs and sperm cells were quantified using a cell counting chamber under a microscope at $200\times$ magnification. The estimated time from sample injection to collection of the processed sample was ~ 5 min, which is more than 10 times shorter than current clinical protocols (density gradient centrifugation).

To visualize the flow focusing of WBCs and sperm cells within the spiral channel, a stained Semen A sample was injected at a flow rate of $0.52 \text{ ml per min}^{-1}$ and observed under a high speed scanner equipped with a microscope (Nikon AR1 confocal microscope). The stained sperm cells were prepared by purifying sperm (from semen) using density gradient centrifugation and then stained with 4',6-diamidino-2-phenylindole (DAPI) (Sigma, MO, USA). WBCs from Semen A (Table I) were stained with PKH26 (Sigma, MO, USA) according to the manufacturer's instructions separately before spiking into Semen A. The microscope objective was focused on a location between the end of the 4th ring of the spiral channel and the outlet area (near outlet, Fig. 2). To observe the flow focusing behavior at each ring of the spiral, two individual locations on each ring (as shown in Fig. 2) were selected for data acquisition. On each acquisition, ~ 5 s (840–1050 frames) were collected and analyzed by projecting all frames from each video onto one image using NIS Elements software. The generated projection images were analyzed for the fluorescence intensity of stained cells, and the data were plotted to show cell locations in the channel. The raw intensity data were acquired sequentially from the inner wall boundary to the outer wall boundary and plotted. A curved data acquisition line was traced

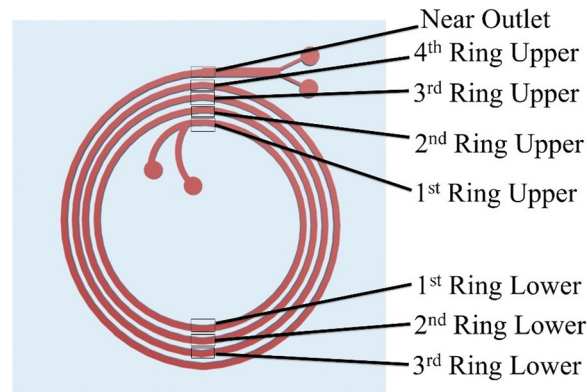


FIG. 2. High-speed camera image acquisition locations to observe the focusing behavior of the cells and their equilibrium positions along the spiral channel (Top view of the spiral channel). Eight different locations were utilized for image acquisition.

along the inner wall boundary and used as an intensity data collection reference. Intensity data along the curved data acquisition line was totaled to determine an accumulated intensity value at a particular position across the channel width. The x axis of the final plot was divided equally into four regions to represent the estimated lateral location of the channel (Inner, Mid-inner, Mid-outer, Outer). The peak location of each cell type was identified using the location of the highest intensity point in the raw data. Note that the 4th ring lower location was considered as redundant with the near outlet area, so the near outlet location represents the last location observed on the 4th ring.

RESULTS AND DISCUSSION

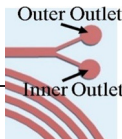
WBC characterization

Experiments with the WBC A (Table I) sample showed flow focusing of WBCs within the spiral channel, and this was confirmed by the WBC count from collected samples at the spiral channel outlets. The results showed that WBCs can be focused under the conditions predicted by theory, as has been shown by others.^{3,45} In Table II, the relative percentage of WBCs directed to the inner outlet was 94.8% ($5.45 \times 10^6/\text{ml}$) or more compared to the outer outlet, which was 5% ($0.3 \times 10^6/\text{ml}$) or less. These results suggest that the WBCs are focusing towards the inner wall with high focusing behavior, as relatively few WBCs strayed to the outer outlet.

Semen A sample characterization

Characterization results using Semen A showed a clear reduction of WBC concentration from the outer outlet while enhancing the sperm concentration from the same outlet (Table II) through clear flow focusing of WBCs and partial flow focusing of sperm cells. WBCs and RBCs primarily exited the inner outlet, while sperm cells were predominantly driven to the

TABLE II. WBC A sample behavior at 0.52 ml/min within the channel.

Cell type	Inner outlet in million/ml (percent of total)	Outer outlet in million/ml (percent of total)	Total in million/ml	Inlet sample in million/ml	
WBC	5.45 ± 0.85 (95%)	0.3 ± 0.1 (5%)	5.75 (100%)	8.1 ± 0.8	
RBC ^a	1.15 ± 0.15 (85.2%)	0.2 ± 0.1 (14.8%)	1.35 (100%)	1.3	

^aRBC count data are included because WBCs were contaminated with some RBCs.

TABLE III. Semen A sample separation results in terms of concentration.

Cell type	Inner outlet in million/ml (percent of total)	Outer outlet in million/ml (percent of total)	Total in million/ml	Inlet sample in million/ml
WBC	7.25 ± 1.63 (92%)	0.47 ± 0.08 (8%)	7.72 (100%)	8.35 ± 0.43
RBC ^a	0.69 ± 0.13 (87.3 %)	0.11 ± 0.05 (12.7%)	0.80 (100%)	1.4 ± 0.05
Sperm	0.58 ± 0.08 (16.8%)	2.81 ± 0.25 (83.2%)	3.39 (100%)	2.45 ± 0.08

^aRBC count data are included, because WBCs were contaminated with some RBCs.

outer outlet. The concentration difference between input and summed outlet samples can be explained by the uncertainty of the cell counting chamber sampling and measurement approach. Detailed results are shown for total concentrations and also percent totals in Table III. The results clearly show that the method is capable of separating out WBCs and RBCs from the majority of sperm cells.

Flow focusing observation of WBCs and sperm cells near the outlet area

Images of the flow focusing behavior of a stained SEMEN A sample [stained WBC (red) and stained sperm (blue)] at the last ring of the spiral channel are shown in Fig. 3. A focused stream of WBCs appeared near the inner wall of the channel and a partially focused stream of sperm appeared in the outer half of the channel. Figure 3 shows the separate and combined images of different constituents during flow. The first image [Fig. 3(a)] shows both the stained WBCs and the sperm cells focused near each outlet mostly in parallel paths. Separate fluorescent signals for sperm cells and WBCs are shown in Figs. 3(b) and 3(c), respectively.

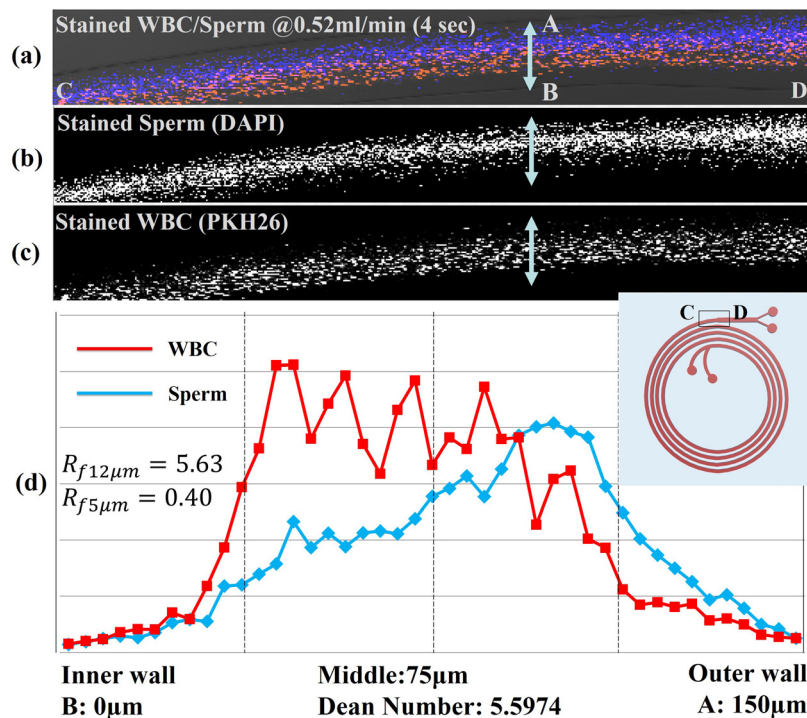


FIG. 3. Results of WBC and sperm location imaging experiments. Each image is a combined stack of frames obtained by high speed camera monitoring near the end of the 4th ring of the channel; (a) combined stained sperm and WBC image; (b) DAPI-only image showing sperm cells; (c) PKH26-only image showing WBCs; (d) optical intensity plot across the width of the channel for the stained sperm cells and WBCs acquired from the obtained images.

Figure 3(c) shows a graph of the fluorescence intensity across the width of the channel and integrated across the breadth for the two cell types. The intensity plot of each signal shows the general location of each cell type relative to one another. The blue plot represents the location of DAPI stained sperm cells, which has its highest intensity peak in the mid outer half of the channel. The red plot represents the location of PKH26 stained WBCs, which has its peak at the middle of the inner half of the channel. These results show a clear shift between the two cell populations, but they are never completely separate, which is consistent with earlier concentration data showing enrichment of sperm cells, but not complete separation.

Flow focusing observation of WBCs and sperm cells in all rings of the channel

The fluorescence images and their intensity profile from locations on all the other rings of the channel are plotted in Fig. 4. These images allow us to visualize the focusing of the sperm cells and WBCs through the channel [Figs. 4(a)–4(h)]. In location a, the intensity of WBCs and sperm cells was evenly spread throughout the channel which represents the evenly suspended condition of the input sample. At location b, the intensity peak of the WBCs begins to narrow in the middle of the channel, but there is limited flow focusing of the sperm cells. Starting at location c, there is a gradual shifting of the signal of the WBC's red fluorescence toward the inner wall of the channel until location h, and the band narrows initially before broadening out close to the exit. This phenomenon can also be seen in each fluorescent intensity plot for each location [Figs. 4(b)–4(h)]. The blue fluorescent signal from the sperm did not show specific signs of focusing until location c, but it is not as highly clustered as the WBC signal at location c. However, the intensity of the blue fluorescent stream gradually moves toward the outer wall

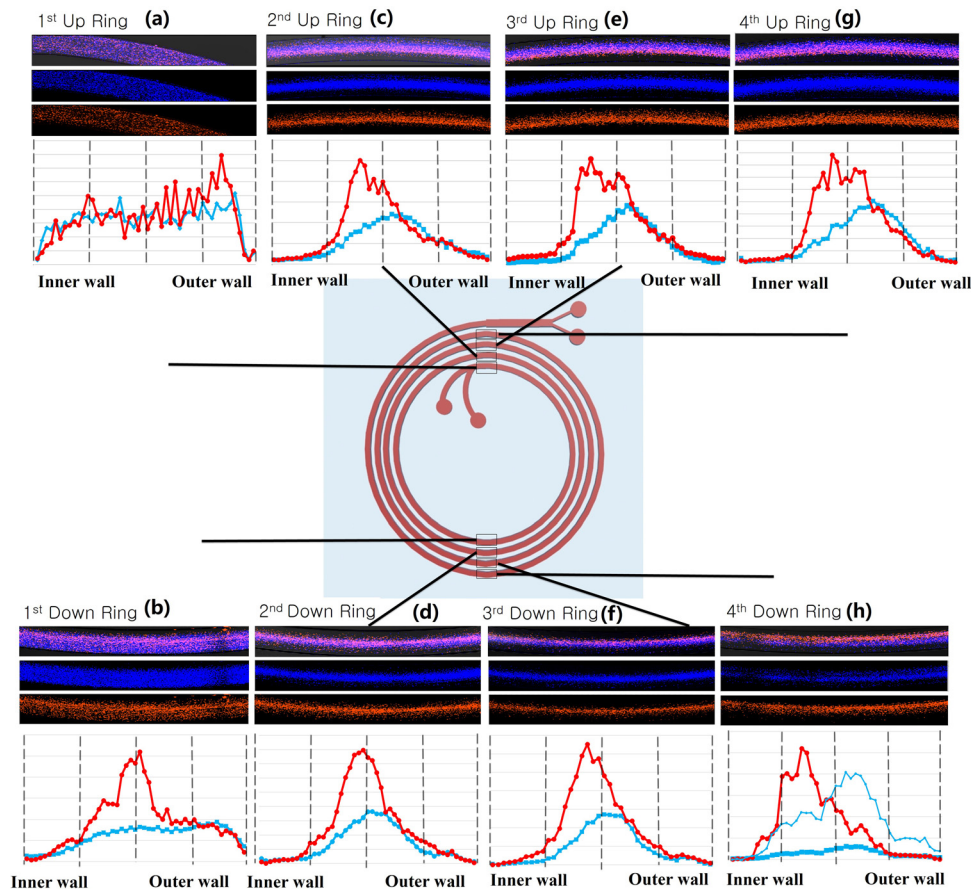


FIG. 4. Stained WBC and sperm flow stacked images and intensity plots at both the “up” and “down” positions of the 1st, 2nd, 3rd, and 4th rings. These positions are expressed as locations (a)–(h).

of the channel from location c to location h [Figs. 3(c)–3(h)]. This transition of the fluorescence intensity of each color (red and blue) gives some insight into the physics affecting these particles. The WBCs, being larger in size, focus more quickly and have a shorter focusing distance along the channel. The sperm cells, being smaller and asymmetric, focus more slowly and do not focus as tightly. The results seem to suggest that the particles reach an equilibrium location by about ring 3, suggesting that the channel could possibly be made shorter. Interestingly, the analysis at the end of the channel and the collected fractions are somewhat different in that the outlet fractions are more fractionated than the images and intensity plots would suggest. Thus, there may be some additional separation that occurs in the brief widening of the channels and split before the outlets.

Equation (5) can be used to calculate a predicted required channel length for reaching the equilibrium position of the WBCs and sperm cells, and these results can be compared to the data in Fig. 4. According to this calculation, R_f (force ratio) for a $12\ \mu\text{m}$ diameter sphere (approximating a WBC) becomes higher than 0.08 by location b: $R_f = 2.42$, and the equilibrium channel length (L_l) for the $12\ \mu\text{m}$ diameter sphere is 0.41 cm, which is 1/10th the length of the first ring. This value of the equilibrium length for WBCs corresponds to the narrowing of the intensity peak of the WBCs at location b, where the channel length is 2.15 cm. From location c, the R_f of $12\ \mu\text{m}$ particle increases from 2.50 to 2.91 until location h, which means that the flow focus of the $12\ \mu\text{m}$ particle should be improved along each ring of the channel. Verifying this prediction with R_f , the red fluorescence signal intensity and peak generally became sharper in the middle of the channel from location c to location f. There are also wider intensity peak profiles at locations e, g, and h. The highest peak in these wider peak profiles seems to move toward the inner wall.

A similar equilibrium length analysis of sperm cells ($5\ \mu\text{m}$ particle) was carried out using Eq. (5) and R_f . The analysis shows that R_f is always above 0.08 (R_f : 0.175 ~0.21) from location a to location h with a flow rate of 0.52 ml/min, which suggests that sperm cells should be focused after location a and the flow focusing should improve while the sperm cells pass through later ring locations. The calculated equilibrium length for a $5\ \mu\text{m}$ particle is 5.73 cm, which occurs between location c and location d. The sperm stream appears to reach its maximum focusing level at this point, and the peak location gradually slides towards a mid-outer location from location d to location h. However, the intensity plot of location h [Fig. 4(h)] again shows that the flow focusing of sperm is not as narrow as the WBC stream.

The analysis of images from Fig. 4 also provides an understanding of the relationship between particle concentration and flow focusing behavior. This phenomenon can be defined by the number of particles per channel length (length fraction),^{34,44} which is defined following the relation: $\beta = 3WHV_f/4\pi a_p^2$. According to Amini *et al.*, in the case of $\beta > 1$, particles cannot be expected to be focused, due to interactions between neighboring particles. Therefore, to minimize interaction between neighboring particles, concentrations of particles should be adjusted to appropriate β values. For this work with $5\ \mu\text{m}$ (sperm: $5 \times 10^6/\text{ml}$) and $12\ \mu\text{m}$ (WBC: $2 \times 10^6/\text{ml}$) diameter particles, $\beta_{5\ \mu\text{m}}$ is 3.6% and $\beta_{12\ \mu\text{m}}$ is 0.6%. For WBC separation by a spiral channel, β is far less than ~50%, which Amini *et al.* described as the threshold of high length fraction. Also, these calculated $\beta_{5\ \mu\text{m}}$ and $\beta_{12\ \mu\text{m}}$ values verify that our initial sample concentration is within the range of the length fraction condition for RBCs (with $\beta_{RBC} = 1.6\%$). Our previous empirical results on the separation of RBCs in spiral channels with $\beta_{RBC} = 1.6\%$ have been reported with good focusing of RBCs.³⁴

It can be observed that the width of focused streams of WBC is not consistent from location a to b. The most focused streams are at locations d and f; wider focused streams are at locations c, e, and g; which are all very similar in width. It seems that this pulsation could be periodic, but additional tests would need to be run to determine if this is a repeatable phenomenon. A plausible explanation for this pulsation of focused streams in Fig. 4 is deformability of WBCs in the flow. A similar effect was also observed by Nivedita and Papautsky in the flow of red blood cells in spiral channels.⁴⁵

In summary, sperm focusing peaks were less sharp than WBC peaks, which is likely due to the asymmetrical shape of the sperm. The results suggest that sperm cells cannot be assumed to

have the same focusing behavior as $5\ \mu\text{m}$ diameter spherical particles, so their effective size must be considered as something smaller. This relatively poor focusing behavior has been briefly discussed by Hur *et al.* in the study regarding inertial focusing of non-spherical micro-particles.⁴² Another helpful report related to the likely behavior of sperm cells in a spiral channel has been presented by Uspal *et al.* in the study regarding engineered self-aligning of particles.⁴⁶ Uspal's study can be used to predict behavior for large aspect ratio particles and may relate to sperm. However, sharp flow focusing of WBCs allowed the significant reduction in the concentration of WBCs in the sample and consequently provided a much cleaner (fewer WBCs) final sample than the initial simulated sample of sperm cells and WBCs.

CONCLUSION

In conclusion, we successfully demonstrated the use of inertial microfluidics to significantly reduce the WBC concentration by flow focusing of WBCs to a waste channel utilizing inertial microfluidic physics. The estimated sample process time was more rapid (~ 5 min) and less hands-on than the conventional method (gradient centrifuge sperm wash; ~ 1 h). A mixture of sperm cells/WBCs was injected as input and 83% of sperm cells and 93% of WBCs were collected separately from two distinct outlets.

During modeling and design preparations, we assumed a spherical shape for WBCs ($12\ \mu\text{m}$ sphere) and sperm cells ($5\ \mu\text{m}$ sphere) and found that the WBC results corresponded with a force ratio (R_f) and equilibrium length typical of a $12\ \mu\text{m}$ sphere particle, suggesting that the modeling of WBCs as a sphere was sufficient, but the results for the sperm cells suggested that modeling them as a $5\ \mu\text{m}$ sphere was not accurate. They were still only modestly focused, suggesting that they behave as smaller particles, or that the asymmetrical nature of the sperm cells causes them to not act like a uniform particle set. Despite the fact that generating sharp flow focusing of sperm was not possible under these conditions, most likely due to our current incomplete understanding of how sperm cells behave in the inertial microfluidic channel, the ability to somewhat focus the sperm cells while sharply focusing the WBCs led to a significant reduction of WBC concentration in pyospermic samples, which should provide a significant advantage over current ART procedures when processing leukospermic samples.

ACKNOWLEDGMENTS

This material is based upon work supported by the National Science Foundation under Grant No. IIP-1549659. The authors would also like to thank the University of Utah Andrology program for their support.

The authors R.S., T.J., B.K.G., D.C., and J.H. declare financial interest in a company, Nanonc, which holds an intellectual property license related to the technology described in this paper.

¹A. A. S. Bhagat, H. W. Hou, L. D. Li, C. T. Lim, and J. Han, "Pinched flow coupled shear-modulated inertial microfluidics for high-throughput rare blood cell separation," *Lab Chip* **11**(11), 1870–1878 (2011).

²M. E. Warkiani *et al.*, "Slanted spiral microfluidics for the ultra-fast, label-free isolation of circulating tumor cells," *Lab Chip* **14**(1), 128–137 (2014).

³T. H. Kim, H. J. Yoon, P. Stella, and S. Nagrath, "Cascaded spiral microfluidic device for deterministic and high purity continuous separation of circulating tumor cells," *Biomicrofluidics* **8**(6), 64117 (2014).

⁴S. Shen *et al.*, "High-throughput rare cell separation from blood samples using steric hindrance and inertial microfluidics," *Lab Chip* **14**(14), 2525–2538 (2014).

⁵M. G. Lee, J. H. Shin, C. Y. Bae, S. Choi, and J. K. Park, "Label-free cancer cell separation from human whole blood using inertial microfluidics at low shear stress," *Anal. Chem.* **85**(13), 6213–6218 (2013).

⁶J. Sun *et al.*, "Double spiral microchannel for label-free tumor cell separation and enrichment," *Lab Chip* **12**(20), 3952 (2012).

⁷L. J. Kricka *et al.*, "Micromachined analytical devices: Microchips for semen testing," *J. Pharm. Biomed. Anal.* **15**(9–10), 1443–1447 (1997).

⁸S. Tasoglu *et al.*, "Exhaustion of racing sperm in nature-mimicking microfluidic channels during sorting," *Small* **9**(20), 3374–3384 (2013).

⁹B. S. Cho, T. G. Schuster, X. Zhu, D. Chang, G. D. Smith, and S. Takayama, "Passively driven integrated microfluidic system for separation of motile sperm," *Anal. Chem.* **75**(7), 1671–1675 (2003).

- ¹⁰T. G. Schuster, B. Cho, L. M. Keller, S. Takayama, and G. D. Smith, "Isolation of motile spermatozoa from semen samples using microfluidics," *Reprod. BioMed. Online* **7**(1), 75–81 (2003).
- ¹¹J. E. Swain, D. Lai, S. Takayama, and G. D. Smith, "Thinking big by thinking small: Application of microfluidic technology to improve ART," *Lab Chip* **13**(7), 1213–1224 (2013).
- ¹²H. Huang, H. T. Fu, H. Y. Tsing, H. J. Huang, C. J. Li *et al.*, "Motile human sperm sorting by an integrated microfluidic system," *J. Nanomed. Nanotechnol.* **5**(3), 199 (2014).
- ¹³H.-Y. Huang *et al.*, "Isolation of motile spermatozoa with a microfluidic chip having a surface-modified microchannel," *J. Lab. Autom.* **19**(1), 91–99 (2013).
- ¹⁴K. Matsuura, M. Takenami, Y. Kuroda, T. Hyakutake, S. Yanase, and K. Naruse, "Screening of sperm velocity by fluid mechanical characteristics of a cyclo-olefin polymer microfluidic sperm-sorting device," *Reprod. Biomed. Online* **24**(1), 109–115 (2012).
- ¹⁵H. Sano, K. Matsuura, K. Naruse, and H. Funahashi, "Application of a microfluidic sperm sorter to the in-vitro fertilization of porcine oocytes reduced the incidence of polyspermic penetration," *Theriogenology* **74**(5), 863–870 (2010).
- ¹⁶J. M. Wu, Y. Chung, K. J. Belford, G. D. Smith, S. Takayama, and J. Lahann, "A surface-modified sperm sorting device with long-term stability," *Biomed. Microdevices* **8**(2), 99–107 (2006).
- ¹⁷L. Xie *et al.*, "Integration of sperm motility and chemotaxis screening with a microchannel-based device," *Clin. Chem.* **56**(8), 1270–1278 (2010).
- ¹⁸Y.-J. Ko, J.-H. Maeng, B.-C. Lee, S. Lee, S. Y. Hwang, and Y. Ahn, "Separation of progressive motile sperm from mouse semen using on-chip chemotaxis," *Anal. Sci.* **28**(1), 27–32 (2012).
- ¹⁹S. Koyama, D. Amarie, H. A. Soini, M. V. Novotny, and S. C. Jacobson, "Chemotaxis assays of mouse sperm on microfluidic devices," *Anal. Chem.* **78**(10), 3354–3359 (2006).
- ²⁰S. S. Suarez and M. Wu, "Microfluidic devices for the study of sperm migration," *Mol. Hum. Reprod.* **23**, 227–234 (2016).
- ²¹C.-Y. Chen *et al.*, "Sperm quality assessment via separation and sedimentation in a microfluidic device," *Analyst* **138**(17), 4967–4974 (2013).
- ²²S. M. Knowlton, M. Sadasivam, and S. Tasoglu, "Microfluidics for sperm research," *Trends Biotechnol.* **33**(4), 221–229 (2015).
- ²³R. Ma *et al.*, "In vitro fertilization on a single-oocyte positioning system integrated with motile sperm selection and early embryo development," *Anal. Chem.* **83**(8), 2964–2970 (2011).
- ²⁴Y. Lin, P. Chen, R. Wu, L. Pan, and F. Tseng, "Micro diffuser-type movement inversion sorter for high-efficient sperm sorting," in *2013 8th IEEE International Conference on Nano/Micro Engineered and Molecular Systems (NEMS)* (2013), pp. 7–10.
- ²⁵M. D. C. Lopez-Garcia, R. L. Monson, K. Haubert, M. B. Wheeler, and D. J. Beebe, "Sperm motion in a microfluidic fertilization device," *Biomed. Microdevices* **10**(5), 709–718 (2008).
- ²⁶M. Wheeler and M. Rubessa, "Integration of microfluidics and mammalian IVF," *Mol. Hum. Reprod.* **23**, 248–256 (2016).
- ²⁷R. S. Suh, X. Zhu, N. Phadke, D. A. Ohl, S. Takayama, and G. D. Smith, "IVF within microfluidic channels requires lower total numbers and lower concentrations of sperm," *Hum. Reprod.* **21**(2), 477–483 (2006).
- ²⁸J. Son, K. Murphy, R. Samuel, B. Gale, D. Carrell, and J. Hotaling, "Non-motile sperm cell separation using a spiral channel," *Anal. Methods* **7**, 8041–8047 (2015).
- ²⁹L. Gambera, F. Serafini, G. Morgante, R. Focarelli, V. De Leo, and P. Piomboni, "Sperm quality and pregnancy rate after COX-2 inhibitor therapy of infertile males with abacterial leukocytospermia," *Hum. Reprod.* **22**(4), 1047–1051 (2007).
- ³⁰C. M. Peterson, A. O. Hammoud, E. Lindley, D. T. Carrell, and K. Wilson, *Assisted Reproductive Technology Practice Management* (Springer, New York, 2010).
- ³¹G. B. Nash, J. G. Jones, J. Mikita, B. Christopheher, and J. A. Dormandy, "Effects of preparative procedures and of cell activation on flow of white cells through micropore filters," *Br. J. Haematol.* **70**, 171–176 (1988).
- ³²M. J. Chen and A. Bongso, "Comparative evaluation of two density gradient preparations for sperm separation for medically assisted conception," *Hum. Reprod.* **14**(3), 759–764 (1999).
- ³³S. S. Kuntaegowdanahalli, A. A. S. Bhagat, G. Kumar, and I. Papautsky, "Inertial microfluidics for continuous particle separation in spiral microchannels," *Lab Chip* **9**(20), 2973–2980 (2009).
- ³⁴H. Amini, W. Lee, and D. Di Carlo, "Inertial microfluidic physics," *Lab Chip* **14**(15), 2739–2761 (2014).
- ³⁵J. Zhou and I. Papautsky, "Fundamentals of inertial focusing in microchannels," *Lab Chip* **13**(6), 1121–1132 (2013).
- ³⁶J. M. Martel and M. Toner, "Inertial focusing dynamics in spiral microchannels," *Phys. Fluids* **24**(3), 32001 (2012).
- ³⁷J. M. Martel and M. Toner, "Particle focusing in curved microfluidic channels," *Sci. Rep.* **3**, 3340 (2013).
- ³⁸P. R. Wheeler, H. G. Burkitt, and V. G. Daniels, *Functional Histology: A Text and Colour Atlas* (Churchill Livingstone, 1979).
- ³⁹M. Diez-Silva, M. Dao, J. Han, C.-T. Lim, and S. Suresh, "Shape and biomechanical characteristics of human red blood cells in health and disease," *MRS Bull.* **35**(5), 382–388 (2010).
- ⁴⁰J. A. Mossman, J. T. Pearson, H. D. Moore, and A. A. Pacey, "Variation in mean human sperm length is linked with semen characteristics," *Hum. Reprod.* **28**(1), 22–32 (2013).
- ⁴¹L. Maree, S. S. Du Plessis, R. Menkveld, and G. Van Der Horst, "Morphometric dimensions of the human sperm head depend on the staining method used," *Hum. Reprod.* **25**(6), 1369–1382 (2010).
- ⁴²S. C. Hur, S. E. Choi, S. Kwon, and D. Di Carlo, "Inertial focusing of non-spherical microparticles," *Appl. Phys. Lett.* **99**(4), 044101 (2011).
- ⁴³J. E. Lackner, I. Märk, K. Sator, J. Huber, and M. Sator, "Effect of leukocytospermia on fertilization and pregnancy rates of artificial reproductive technologies," *Fertil. Steril.* **90**(3), 869–871 (2008).
- ⁴⁴D. Di Carlo, "Inertial microfluidics," *Lab Chip* **9**(21), 3038–3046 (2009).
- ⁴⁵N. Nivedita and I. Papautsky, "Continuous separation of blood cells in spiral microfluidic devices," *Biomicrofluidics* **7**(5), 054101 (2013).
- ⁴⁶W. E. Uspsal, H. Burak Eral, and P. S. Doyle, "Engineering particle trajectories in microfluidic flows using particle shape," *Nat. Commun.* **4**, 2666 (2013).